JOURNAL OF GUIDANCE, CONTROL, AND DYNAMICS
Vol. 15, No. 4, July-August 1992

High Performance, Accelerometer-Based Control of the Mini-MAST Structure

Emmanuel G. Collins Jr.,* James A. King,† Douglas J. Phillips,‡ and David C. Hyland§
Harris Corporation, Melbourne, Florida 32902

Many large space system concepts will require active vibration control to satisfy critical performance requirements such as line-of-sight pointing accuracy and constraints on rms surface roughness. For these concepts to become operational, it is imperative that the benefits of active vibration control be practically demonstrated in ground-based experiments. This paper describes an experiment conducted on the Mini-MAST test bed, a structure located at NASA Langley Research Center that has features dynamically traceable to future space systems. The results of this experiment demonstrate the successful application of a modern control design methodology to active vibration control for a flexible structure. To maximize traceability to current flight system technology, the controllers were designed and implemented using sensors (four accelerometers and one rate gyro) that are actually mounted to the structure.

I. Introduction

MANY future space missions will require active vibration control to satisfy critical performance requirements such as line-of-sight pointing accuracy and constraints on rms surface roughness. An important step in the development of this technology is demonstration in ground-based experiments. This paper discusses an experiment conducted on the Mini-MAST test bed at NASA Langley Research Center. This experiment required control design and implementation for the Mini-MAST structure and successfully demonstrated active structural control technology. References 1 and 2 describe the application of a similar methodology to control design for the Active Control Evaluation for Spacecraft (ACES) structure at NASA Marshall Space Flight Center.

The Mini-MAST structure, shown in Fig. 1, is a beamlike truss structure. This structure can be viewed as the secondary support tower of a precision optical structure. To achieve high-accuracy line-of-sight pointing in such a structure, it is important to minimize the relative displacement of the tip of the beam with respect to the base. Hence, the primary objective of this experiment was to design controllers that provide substantial reduction of the displacement of the tip of the Mini-MAST structure. Particular emphasis was also placed on controller simplicity (i.e., decentralized and reduced-order controller architectures). Complexity reduction in control law implementation is of paramount interest due to stringent limitations on throughput of even state-of-the-art space-qualified processors.

To maximize traceability to current flight system technology, only the (acceleration and rate) sensors that are mounted on the Mini-MAST structure were used. Five sensors were used: four accelerometers and one rate gyro. Ground-mounted displacement sensors were available but were used only for performance evaluation.

The performance objective required control of the low-frequency modes without destabilizing the higher-frequency modes (which is a standard structural control problem). Because of the use of accelerometers, which tend to emphasize higher-frequency modes more than do displacement or rate sensors, it was very important to ensure that the control laws rolled off sufficiently to avoid destabilizing the higher-frequency modes. In this experiment, the rolloff was enforced by using a precompensation strategy. That is, practical rolloff filters were first designed using classical insights and included as part of the plant. Linear quadratic Gaussian (LQG) and full-order maximum entropy control laws[3-7] were designed using the modified plant. The order of these controllers was then reduced using balanced controller reduction.[8] The rolloff filters were then appended to the reduced-order LQG and maximum entropy control laws to obtain the control laws that were actually implemented. As will be seen in the subsequent results, this methodology proved to be very effective for achieving the control design objectives for the Mini-MAST.

The paper is organized as follows. Section II provides a brief description of the Mini-MAST test bed and describes the Mini-MAST models provided by NASA Langley. Section III reviews maximum entropy control design. Section IV defines the basic control design problem and discusses the precompensation methodology used for control design. Section V describes the control design strategy used in this experiment and the reduced-order models that were used to develop the control laws. This section also discusses some of the key design details such as the dynamics of the precompensator filters and the weighting schemes that were used. Sections VI and VII describe, respectively, the decentralized and centralized designs that were implemented and the resultant performance improvement. Finally, Sec. VIII presents the closing discussion.

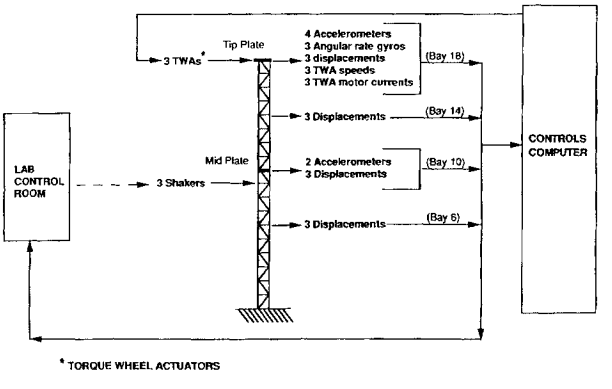

Fig. 1 Mini-MAST test article.

Received April 16, 1991; revision received Nov. 1, 1991; accepted for publication Nov. 14, 1991.

*Associate Principle Engineer, Government Aerospace Systems Division.
†Senior Engineer, Government Aerospace Systems Division.
‡Staff Engineer, Government Aerospace Systems Division.
§Senior Scientist, Government Aerospace Systems Division.

II. Description of the Mini-MAST Test Article and Models

This section provides a brief description of the Mini-MAST experimental test bed, located at NASA Langley Research Center. A more detailed description is provided in Ref. 9.

The basic Mini-MAST test article is a generic space truss designed and manufactured by Astro Aerospace Corporation. The tubing members of the truss are made of graphite epoxy. The truss beam is deployable and retractable and has a triangular cross section. The total height of the truss is 20.16 m and the truss consists of 18 bays, each of which is 1.12 m in height.

The actuators and sensors available for control design implementation, disturbance generation, and performance evaluation are shown in Fig. 1. The only actuators available for control are three torque wheel actuators that are mounted on the tip plate (top of bay 18) parallel to the global x, y, and z reference axes. The torque wheels provide both torsional and bending torque loads to the Mini-MAST. These dc permanent-magnet motors have a rated peak output of 50 ft-lbs at 50 V and 9.6 A.

The available control sensors are six Sundstrad QA-1400 servo accelerometers and three Watson angular rate gyros. Four accelerometers are located at the beam tip (bay 18) and two are located on the midplatform (bay 10). These sensors measure linear acceleration in the global x and y directions. The three rate sensors are located at the beam tip (bay 18) and measure pitch (about the x axis), roll (about the y axis), and yaw (about the z axis).

Fifty-one Kaman KD-230 proximity probes (i.e., displacement sensors) are installed on the support structure along the Mini-MAST. These devices can be used for control but were primarily intended for structural dynamic testing and performance evaluation. Our experimentation used the three Kaman sensors at bay 18 for performance evaluation. These sensors are oriented normal to the faces of the truss at each of the three vertices.

Three Unholtz-Dickie 50-lb shakers are attached at bay 9 for disturbance generation. These shakers have the same orientation as the Kaman sensors at bay 18.

Two models of the Mini-MAST were provided by NASA Langley Research Center. The first model was used to generate the reduced-order models that were used to design the decentralized controllers and had good correspondence to experimental data below 10 Hz. A second model that had even better correspondence to experimental data under 10 Hz was provided later in the program and was used to generate the reduced-order model that was used to design the centralized controllers. The final evaluation model for each of the control designs was the full-order second model, discretized at 80 Hz, the sample frequency chosen for control law implementation. Delay states were included in the evaluation model to account for the one sample period computational delay.

Both of the models consisted of essentially three parts: the torque wheel dynamics, the finite element generated structural dynamics, and the 20-Hz analog Bessel filters used to filter the sensor outputs. The dynamics of the three torque wheels were quite similar to one another and significantly contributed to the plant dynamics over a wide bandwidth. For example, the dynamics of torque wheel X provided 75 deg of phase lead at 0.8 Hz, the frequency of the first bending modes, and provided a magnitude variation of over 50 dB from 1 to 100 Hz. The 20-Hz Bessel filters were chosen instead of lower-frequency Bessel filters to allow better control of the second bending modes, which had frequencies of around 6 Hz. Only one shaker at bay 9, shaker A, was used to disturb the structure, and the three Kaman sensor measurements at bay 9, displacements A, B, and C of bay 18, were used for performance evaluation. The inputs used for control law implementation were the three torque wheels at bay 18—torque X, torque Y, and torque Z. The outputs used were two bay 18 accelerometers—acceleration 1X and acceleration 2Y; the bay 10 accelerometers—acceleration X and acceleration Y; and the torsional rate gyro at bay 18—rate gyro Z. As opposed to model 1, which contained 18 structural modes, the structural dynamics for model 2 were composed of 28 modes. Most of the additional modes are a set between 15–20 Hz, involving the diagonal members and the tip plate.

The first five modes of model 2 were as follows. The first two modes were both at 0.83 Hz and were the first bending modes in the X and Y directions. The third mode was the first torsional mode (at 4.37 Hz). The next two modes were the second bending modes in the X and Y directions and were located at 6.44 and 6.38 Hz, respectively. This model contained 23 additional modes from 14.72 to 73.34 Hz.

III. Maximum Entropy Design

The maximum entropy approach to control design was developed particularly to allow high-performance robust control law design for flexible structures and appears to be closely related to recent results on parameter-dependent Lyapunov functions and variations of the Popov criterion.[10] Maximum entropy design[3–7] assumes an uncertain plant of the form

$$\dot{x}(t) = (A + \Delta A)x(t) + Bu(t) + D_1 w_1(t) \tag{1}$$

$$y(t) = Cx(t) + w_2(t) \tag{2}$$

$$z(t) = E_1 x(t) \tag{3}$$

where $x \in \mathcal{R}^{n_x}$, $u \in \mathcal{R}^{n_u}$, $y \in \mathcal{R}^{n_y}$, $z \in \mathcal{R}^{n_z}$, $w_1 \in \mathcal{R}^{n_w}$ is white disturbance noise with non-negative definite intensity V_1, $w_2 \in \mathcal{R}^{n_y}$ is white observation noise with positive definite intensity V_2, and w_1 and w_2 are uncorrelated. The state matrix A is assumed to be in real normal form such that A is block diagonal with scalar blocks corresponding to the real poles of the system and 2×2 blocks of the form

$$\begin{bmatrix} -\nu_i & \omega_i \\ -\omega_i & -\nu_i \end{bmatrix}$$

corresponding to the flexible modes. It is assumed that the uncertainty ΔA is of the form

$$\Delta A = \sum_{i=1}^{n_\alpha} \delta_i A_i, \qquad |\delta_i| \le \alpha_i, \quad \alpha_i \ge 0 \tag{4}$$

where n_α denotes the number of uncertain modes, and each A_i is of the form

$$A_i = \text{block diag}\left\{0,\ldots,0,\begin{bmatrix} 0 & 1 \\ -1 & 0 \end{bmatrix},0,\ldots,0\right\} \tag{5}$$

corresponding to uncertainty in ω_i, the frequency of the ith mode.

Full-order maximum entropy design allows the synthesis of an n_xth-order dynamic compensator,

$$\dot{x}(t) = A_c x_c(t) + B_c y(t) \tag{6}$$

$$u(t) = -C_c x_c(t) \tag{7}$$

that minimizes the steady-state performance criterion

$$J(A_c,B_c,C_c) \triangleq \lim_{t\to\infty} E\left[x^T(t)R_1 x(t) + u^T R_2 u(t)\right]$$

$$R_1 = E_1^T E_1, \qquad R_2 > 0 \tag{8}$$

subject to a constraint on a modified closed-loop Lyapunov equation, which is a function of δ_i and A_i.[6,7] The computation of the maximum entropy controller requires solving a set of four coupled equations: two Riccati equations and two Lyapunov equations. These equations can be solved using a homotopy algorithm.[5] If we assume perfect knowledge of the system

(i.e., $\delta_i = 0$ for $i = 1, \ldots, n_\alpha$), then the four equations decouple and the Riccati equations become the standard LQG Riccati equations.

IV. Problem Definition and the Introduction of a Precompensation Methodology for Control Design

As mentioned in the Introduction, the basic control objective was to minimize the displacements at the tip of the Mini-MAST. It was assumed that the Mini-MAST would be subjected to a 0.1-s pulse of 50-N amplitude from shaker A. It was evident from the magnitude Bode plots from shaker A to displacements A, B, and C of bay 18 that, if shaker A is used to excite the Mini-MAST with a pulse of infinitesimal duration, then the open-loop displacements at the tip are primarily due to the excitation of the first bending modes of the X and Y axes (at 0.8 Hz) with minor contributions from the first torsional mode (at 4.4 Hz) and the second bending modes of the X and Y axes (at 6.1 and 6.2 Hz). Since the disturbance pulse was actually of finite duration, the contributions of the latter three modes were even further reduced.

From this analysis it was apparent that the performance objectives required the control of no more than five modes with the first bending mode pair being the two most important modes to attenuate. The control design thus required the control of these five modes without destabilizing the remaining higher-frequency modes, all of which are above 14 Hz. Recognize that the experimental data discussed in Sec. II that was used to verify the accuracy of the two models was only valid below 10 Hz. Thus, we did not have confidence in our models above 10 Hz and wished to ensure stability of these modes by having the compensators roll off these modes to achieve gain stabilization.

An additional motivation for using a rolloff strategy for achieving the desired high-frequency stabilization was that we used continuous-time models and design theory for the control designs. The controllers were then discretized for implementation at 80 Hz. This discretization tends to distort the higher-frequency dynamics of the continuous-time compensators, which can cause instability when the discretized controllers are implemented. The use of compensator rolloff for high-frequency stabilization was used to reduce the importance of high-frequency compensator dynamics.

It is important to note that, for this problem, the desired rolloff could not be achieved by a straightforward application of LQG design theory. This fact is illustrated by Fig. 2, which shows an LQG compensator designed using a reduced-order model of the torque X to acceleration 2Y transfer function. The reduced model included only one mode above 10 Hz, a 20.3-Hz mode. The LQG compensator was designed to attenuate the first bending mode at 0.8 Hz. The compensator

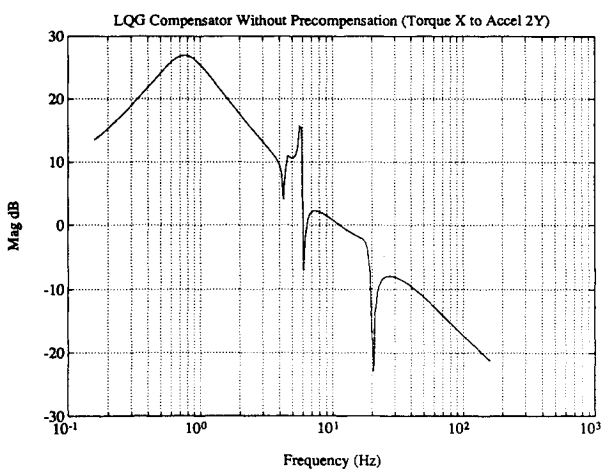

Fig. 2 Frequency response magnitude of an LQG compensator designed without using precompensation.

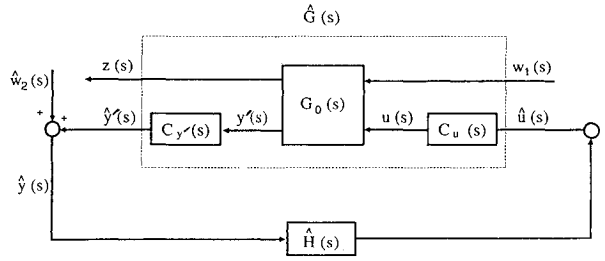

Fig. 3 Design configuration for the precompensation methodology.

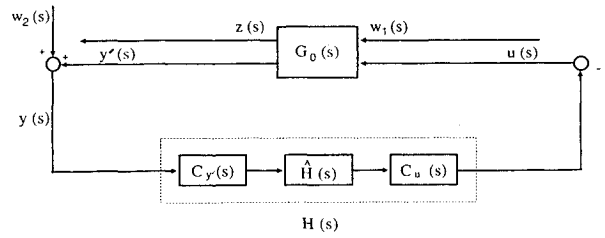

Fig. 4 Implementation configuration for the precompensation methodology.

shown in Fig. 2 has sufficient gain at the first bending mode to achieve significant performance improvement, but the gain stabilizes the 20-Hz mode by notching it and has enough gain above 20 Hz to potentially destabilize the unmodeled modes. This type of compensator was clearly undesirable.

The desired rolloff could have been ensured by assuming norm-bounded uncertainty and using either H_∞[11-16] or μ-synthesis[17,18] control design. Alternatively, one could have used frequency weighted LQG[16,19,20] to attempt to achieve the desired rolloff. In this experiment, a precompensation strategy was used, which, like frequency weighted LQG, is heuristically based. However, the precompensation methodology does have some attractive features. In particular, it avoids the great increase in dimensionality of the design model that is sometimes resultant from using H_∞, μ synthesis, or frequency weighted LQG methods. Also, this methodology is very easy to implement.

The basic idea behind the precompensation methodology is very simple and is illustrated in Figs. 3 and 4. As shown in Fig. 3, one simply embeds the precompensation filters (in this case, rolloff filters) $C_u(s)$ and $C_{y'}(s)$ in the plant a priori and designs the modern controller (e.g., an LQG or maximum entropy) $\hat{H}(s)$ for this modified design plant. Then, as illustrated in Fig. 4, the precompensation dynamics are included in the implemented compensator $H(s)$. It is not difficult to show that the closed-loop transfer function $G_{cl}(s)$ satisfying

$$\begin{bmatrix} z(s) \\ y'(s) \end{bmatrix} = [G_{cl}(s)] \begin{bmatrix} w_1(s) \\ u(s) \end{bmatrix} \tag{9}$$

is identical in Figs. 3 and 4. Hence, this methodology ensures that if $\hat{H}(s)$ is stabilizing in the feedback loop of Fig. 3, then $H(s)$ is stabilizing in the feedback loop of Fig. 4. In addition, Eq. (9) also guarantees that the transfer function between $z(s)$ and $w_1(s)$ is preserved, thus ensuring the preservation of attenuation from w_1 to z. However, it is necessary to check after the design process as to whether the compensator achieved the desired rolloff (or robustness to high-frequency unstructured uncertainty). The actual rolloff filters used are described in the next section. This precompensation was also used in the design of controllers for an important benchmark problem.[21]

V. Control Design Strategy and Models

A very practical control design and implementation strategy was used in this experiment. First, controllers with simple

architectures (i.e., controllers that are decentralized, reduced order, and use few sensors) were developed. Decentralized designs are more desirable for actual flight implementation because they ease the processor requirements, but can be more difficult to design because decentralization requires a careful analysis of the physics of the structure. Subsequently, centralized control laws were developed in an attempt to improve the performance. The centralized design with the best performance did significantly improve the performance of the best decentralized design.

The subcontrollers of the decentralized designs were each single input, single output (SISO). Although the advantages usually stated for modern control usually center around multi-input, multi-output (MIMO) control problems, there are also advantages for SISO systems. In particular, whereas classical control design relies heavily on the designer's intuition and experience to design the feedback filter and is very iterative, modern control helps to automate the design of the feedback filter, generating a filter, which for many problems (including the problem considered here), is in a meaningful sense optimal. In addition, modern control methods do generalize naturally to MIMO control problems. Hence, in a strategy that employs first decentralized control (involving possibly SISO control design) and then centralized (MIMO) control, it is natural to make primary use of one design tool.

The transfer function from torque Z to rate gyro Z was dominated by the first torsional mode at 4.4 Hz. Hence, it appeared feasible to use simple decentralized constant gain feedback from rate gyro Z to torque Z to achieve high attenuation of the torsional mode. A full-order discrete-time model of the system was developed using model 1 to represent the system at the 80-Hz sampling frequency. This model was used to perform a root locus, and it was determined from this root locus that the optimal gain was $K = 10$. All of the implemented controllers were designed assuming that this feedback loop was closed. These designs added feedback loops that use only the accelerometers and the X and Y torques. The use of the rate gyro Z to torque Z feedback essentially eliminated the influence of the torsional mode on the remaining loops, as illustrated by the dotted line in Fig. 5. The resultant performance improvement in the torsional motion is shown in Fig. 6.

Next, we considered controlling the first bending modes in each axis by feeding back accelerometer outputs to the X and Y torque wheels. Since acceleration 1X and acceleration 2X provided essentially the same information about the acceleration of the Mini-MAST tip in the X direction, we decided to use only one of these accelerometers: acceleration 1X. Likewise, we chose to use acceleration 2Y instead of both acceleration 2Y and acceleration 1Y. The remaining accelerometers,

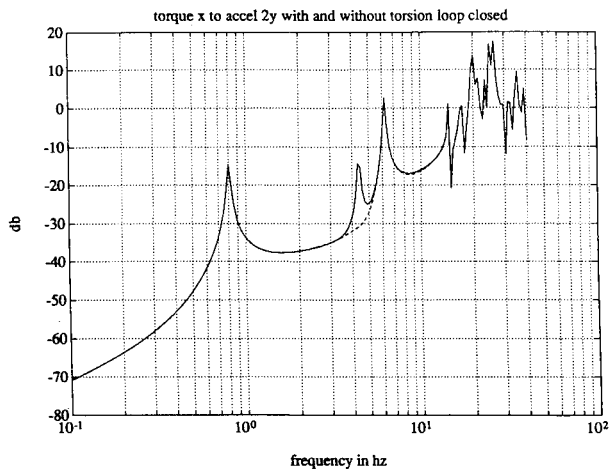

Fig. 5 Effectiveness of constant gain rate feedback in eliminating the influence of the torsional mode (without feedback = solid; with feedback = dashed).

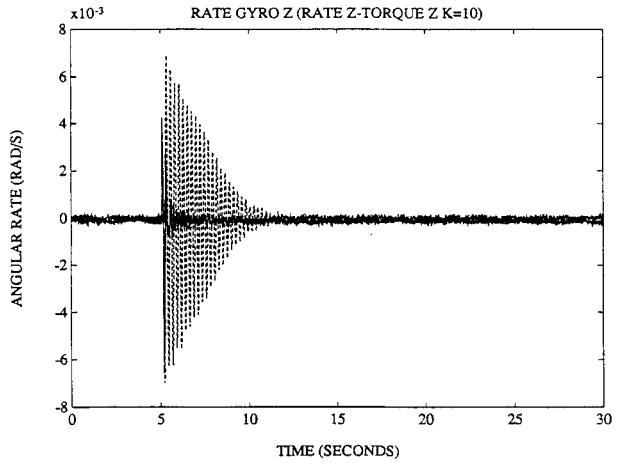

Fig. 6 Open- vs closed-loop rate gyro Z response for constant gain feedback from rate gyro Z to torque Z.

acceleration X and acceleration Y, were located near the center of the Mini-MAST at bay 10.

It was apparent from the frequency responses of the models that the first bending modes were not very prominent in the four transfer functions from torque X and torque Y to acceleration X and acceleration Y. However, the first bending modes were prominent in the four transfer functions from torque X and torque Y to acceleration 1X and acceleration 2Y. Hence, we initially chose to feed back only the latter two accelerometers to control the first bending mode. Furthermore, it was evident that the dominant transfer functions were from torque X to acceleration 2Y and torque Y to acceleration 1X. We thus chose to design feedback laws for the two loops corresponding to these transfer functions.

Reduced-order continuous-time models were developed for the transfer functions torque X to acceleration 2Y and torque Y to acceleration 1X. First-order all-pass filters were included in each model to account for the phase lag due to the one sample period computational delay. Precompensation dynamics were added to each reduced-order model to yield the models actually used to design the reduced-order LQG and maximum entropy controllers. The torque X to acceleration 2Y design model and the torque Y to acceleration 1X design model each contained 20 states.

The precompensation for each of the two control problems was chosen so that the modified design plant appeared to have a rate measurement and a true torque input within the control bandwidth. The precompensation thus consisted of dynamics to integrate the accelerometer output and dynamics to cancel the effects of the actuator dynamics below 10 Hz. This choice of precompensation added the desired rolloff to the original design plant and also allowed us to develop a baseline rate-feedback design. Because the transfer functions for each of the two control problems were so similar, we decided to use the same precompensation for both. Referring to Fig. 3, the precompensation used is given by

$$C_u(s) = \frac{s + 62.8}{s^2 + 0.628s + 0.3944}, \qquad C_{y'}(s) = 1 \tag{10}$$

Because of the requirements of maximum entropy design, each of the modified design models was placed in real normal form. Thus, the A matrix of each of the modified design models was block diagonal with one of the blocks of the form

$$\begin{bmatrix} -\nu_1 & \omega_1 \\ -\omega_1 & -\nu_1 \end{bmatrix}$$

corresponding to the first bending mode. The disturbance weighting matrix V_1 and the performance state weighting ma-

trix R_1 were each chosen to be block diagonal with the only nonzero block corresponding to the position of the first bending mode in the A matrix. The nonzero block of V_1 is given by

$$\begin{bmatrix} 0 & 0 \\ 0 & \alpha \end{bmatrix}$$

and the nonzero block of R_1 is given by

$$\begin{bmatrix} \alpha & 0 \\ 0 & 0 \end{bmatrix}$$

where α is a scalar parameter that was used to determine the controller authority. This choice of weighting matrices was equivalent to assuming that the system was disturbed by a force actuator and the performance output was a displacement sensor that sees only the first bending mode when an impulse is placed in the system by the force actuator. Also, we chose $R_2 = V_2 = 1$.

The centralized designs used a reduced-order continuous-time model that contained 12 structural modes. This model also included first-order all-pass filters to account for the phase lag due to the one sample period computational delay. Precompensation dynamics were added to the reduced-order model, which yielded a design model with 54 states.

It should be noted that each of the models used for (centralized or decentralized) control design included modes with frequencies above the first five modes in the bandwidth of interest. These modes were included to increase the accuracy of the first five modes in the reduced-order design model. That is, if none of the higher-frequency modes were included, the phases and magnitudes of the first five modes were significantly distorted.

The precompensation dynamics that we used for the centralized controllers differed from that used for the decentralized controllers. The reason for this change was primarily an attempt to eliminate some of the low-frequency oscillation that appeared in the output of the displacement sensors and ultimately limited the achievable performance of the decentralized designs. We initially attributed this low-frequency oscillation to the migration of the low-frequency poles of the precompensation dynamics toward the right half-plane, although subsequent control design and analysis revealed that this was not actually the case. Referring again to Fig. 3, the precompensation used is given by

$$C_u(s) = \text{diag}\{C_{u,1}(s), C_{u,2}(s)\}, \qquad C_{y'}(s) = I \tag{11}$$

where

$$C_{u,1}(s) = C_{u,2}(s) = \frac{39.0625 \times 10^4}{(s^2 + 18.8755 + 62.5)(s^2 + 45.969 + 625)} \tag{12}$$

$C_{u,1}(s)$ and $C_{u,2}(s)$ are 4-Hz Butterworth filters and, hence, provide rolloff between the first and second bending modes.

The weighting scheme used for the centralized controllers is very straightforward. Let the state-space representation corresponding to the modified design plant $\hat{G}(s)$ in Fig. 3 be given by

$$\dot{x}(t) = Ax(t) + B\hat{u}(t) + D_1 w_1(t) \tag{13}$$

$$\hat{y}(t) = Cx(t) + \hat{w}_2(t) \tag{14}$$

$$z(t) = E_1 x(t) \tag{15}$$

where the basis of Eqs. (13-15) is chosen such that A is in real normal form. Here, it is assumed that $w_1 \in \mathfrak{R}$ denotes the input corresponding to shaker A and

$$z = \begin{bmatrix} z_a \\ z_b \end{bmatrix}, \qquad E_1 = \begin{bmatrix} E_{1,a} \\ E_{1,b} \end{bmatrix} \tag{16}$$

where $z_a \in \mathfrak{R}^3$ denotes a performance vector whose elements correspond to displacements A, B, and C of bay 18; and $z_b \in \mathfrak{R}^3$ denotes the performance vector whose elements correspond to displacements A, B, and C of bay 10. The weights R_1, R_2, V_1, and V_2 in the control problem of Sec. III were chosen as

$$R_1 = \alpha E_{1,a}^T E_{1,a} + \beta E_{1,b}^T E_{1,b}, \qquad V_1 = \alpha I, \qquad R_2 = V_2 = 1 \tag{17}$$

where the scalar parameter α was used to determine the controller authority. The scalar parameter β was chosen to be zero for the initial designs but was given a finite value in later designs in order to penalize the bay 10 displacements. The use of the parameter β was motivated by the fact that the dominant behavior at bay 10 was due to the second bending mode pair. Thus, β was essentially used to reduce the influence of the second bending modes on the displacement responses at bay 18.

VI. Decentralized Control Designs

This section describes in more detail the decentralized controllers discussed in the previous section and presents the resultant performance improvement. Four controllers are described, each of which was designed using the precompensation methodology of Sec. IV. Each controller was also designed assuming that a decentralized constant gain feedback loop from torque Z to rate gyro Z (with gain $K = 10$) was closed. This feedback loop essentially eliminated the effects of the first torsional mode. Hence, although the controllers described used only acceleration 1X, 2Y, X, and Y for sensing and torques X and Y for actuation, it is important to keep in mind that they were implemented in conjunction with the constant gain feedback law from torque Z to rate gyro Z.

Each of the four decentralized controllers included at least two subcontrollers, one fed back acceleration 2Y to torque X, whereas the other fed back acceleration 1X to torque Y. These two subcontrollers were designed using the precompensation methodology of Sec. IV with precompensation dynamics given by Eqs. (10). Controller 1 consisted of two subcontrollers. Referring to Fig. 3, these subcontrollers were designed by simply choosing $\hat{H}(s)$ equal to a constant. Since the precompensation was chosen to make the design plants $\hat{G}(s) \triangleq C_{y'}(s)G(s)C_u(s)$ for each subcontroller appear to have a rate measurement and a true torque input within the control bandwidth, controller 1 approximated a rate feedback controller and was used as a baseline design. Controller 2 also included only two subcontrollers and was designed without assuming uncertainty in any of the first five modes. Controller 3 was similar to controller 2 except that it was designed assuming uncertainty in the second bending mode pair. Controller 4 consisted of controller 3 plus two additional subcontrollers designed using classical control concepts that fed back accelerometers at bay 10. One of these subcontrollers fed back acceleration Y to torque X, whereas the other subcontroller fed back acceleration X to torque Y. The subcontrollers were discretized using the bilinear transformation with frequency prewarping to match the continuous-time and discrete-time representations of the subcontroller at the frequency of the second modes (about 6 Hz). At implementation, the gain of each of the five decentralized controllers was increased as much as possible to maximize the performance.

Controller 1: Pseudo-rate Feedback Controller

This controller consisted of two subcontrollers, one from acceleration 2Y to torque X and one from acceleration 1X to torque Y. This controller was our least complex and, as previously mentioned, was used as a baseline design. Although this controller did provide substantial increase in the performance, it will subsequently be seen that more complex controllers achieved much better performance.

Controller 2: Reduced-Order Linear Quadratic Gaussian Controller Using Bay 18 Accelerometers

Like controller 1, this controller consisted of two subcontrollers, one from acceleration 2Y to torque X and one from acceleration 1X to torque Y. However, the feedback laws in this case were designed using LQG. The decentralized feedback laws for each loop were each of order 9 (including the precompensation) so that the implemented controller was of order 18.

Controller 3: Reduced-Order Maximum Entropy Controller Using Bay 18 Accelerometers

This controller was a robustified version of controller 2 and was of order 20. It was designed assuming uncertainty in the second bending mode pair and, as illustrated by Fig. 7, the maximum entropy design robustified the corresponding notches for these two modes. This uncertainty description was originally motivated by an analysis of controller 2, which indicated that the controllers were sensitive to uncertainties in the second bending modes. However, due to the high fidelity of the models provided by NASA, subsequent analysis revealed that robustness was not really needed. Nevertheless, the maximum entropy design yielded useful gain margin at the frequency of the second bending modes and allowed us to scale the subcontrollers to further attenuate the influence of the first bending modes on the performance. Also, note that the small 20-Hz notch appearing in Fig. 7 was not needed to gain stabilize the corresponding 20-Hz plant mode. This notch appeared solely as a consequence of optimality and contrasts with the large 20-Hz notch of Fig. 2, which was needed to gain stabilize the corresponding plant mode.

Controller 4: Controller 3 Plus a Classical Controller Using Bay 10 Accelerometers

This controller consisted of controller 3 plus two simple subcontrollers, $H_1(z)$ and $H_2(z)$, which were designed using classical control concepts. $H_1(z)$ was used in the feedback path from acceleration Y to torque X, and $H_2(z)$ was used in the feedback path from acceleration X to torque Y. These two subcontrollers were designed to further attenuate the second bending modes and are given, respectively, by

$$H_1(z) = K_1 z/(z-0.9245)$$

$$H_2(z) = K_2 z/z(z-0.9245)^2$$

where K_1 and K_2 are constant gains. The implemented compensator was of order 24. It should be noted here that the only reason that all other controllers were designed in the s domain was the greater maturity of the theory and design tools available for continuous-time robust control. Classical control was used here because of the simplicity of the design problem.

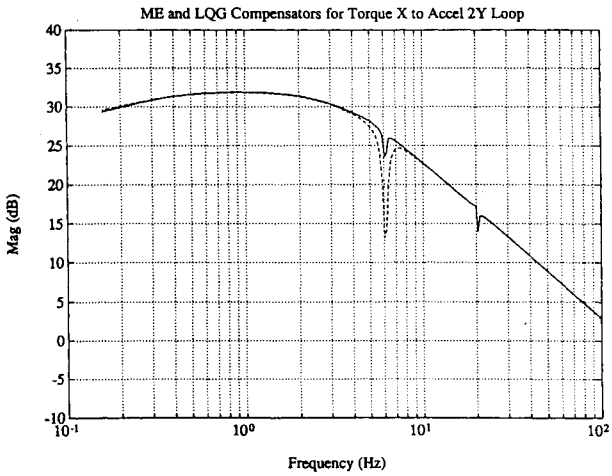

Fig. 7 Comparison of the magnitude Bode plots for the acceleration 2Y to torque X $\hat{H}(s)$ subcontroller of controller 2 and 3 (controller 2 = solid; controller 3 = dashed).

Figure 8 shows the performance for each of the controllers as evidenced from displacement A of bay 18. The results were very close to the predicted results. As desired, each successive controller improved on the performance of the prior controllers.

VII. Centralized Controllers

This section further describes three of the centralized controllers discussed in Sec. V and presents the resultant performance improvement for each controller. As was the case for the decentralized controllers, controllers 1-4, each of these centralized controllers was designed assuming that a decentralized constant gain feedback loop from torque Z to rate gyro Z (with gain $K = 10$) was closed, which effectively eliminated the effects of the first torsional mode. These controllers were designed after the decentralized controller experiments had been performed. It was during those experiments that we discovered we could rely more on the provided models (below 10 Hz) and that robustness in the control bandwidth was not a significant issue.

Each of the five controllers was designed using the precompensation methodology of Sec. IV with precompensation dynamics given by Eqs. (11) and (12). The design weights are given by Eqs. (17), with α and β being the design parameters. The first centralized controller, controller 5, fed back bay 18 acceleration 2Y and 1X to torques X and Y. Controllers 6 and 7 also fed back bay 10 acceleration Y and X to torques X and Y. The difference between these two controllers was due to the amount of performance penalty that was placed on the displacements at bay 10. None of these latter three controllers was designed assuming uncertainty in the first five modes. The controllers were discretized using the bilinear transformation with frequency prewarping to match the continuous-time and discrete-time representations of the controller at the frequency of the second bending modes (about 6 Hz). As with the decentralized controllers, at implementation, the gain of each of these controllers was increased as much as possible to maximize the performance.

It is of interest to note that, although the centralized controllers were designed assuming 20-Hz Bessel filters to process the sensor outputs, each of the controllers was originally inadvertently implemented with 10-Hz Bessel filters, which provided substantial phase delay in the controller bandwidth. Nevertheless, each controller was able to stabilize the system and obtain substantial performance improvement after the controller gain was reduced by a factor of 2. In addition, one of the controllers, controller 6, was stabilizing without reducing its gain.

Controller 5: Reduced-Order Linear Quadratic Gaussian Controller Using Bay 18 Accelerometers

This controller was the least complex centralized controller that was implemented and was designed to feed back acceleration 2Y and 1X to torques X and Y. The displacements at bay 10 were not penalized in the design process [i.e., $\beta = 0$ in Eqs. (17)]. No uncertainty was assumed in the first five modes. The controller is of order 26. The performance of this compensator, which uses two sensors, was comparable to the performance of controller 4, a decentralized controller that used four sensors, and had better performance than the decentralized controllers using only the two sensors employed by controller 5.

Controller 6: Reduced-Order Linear Quadratic Gaussian Controller Using Bay 10 and Bay 18 Accelerometers

This controller was designed to feed back acceleration 2Y, 1X, X, and Y to torques X and Y. The displacements at bay 10 were not penalized in the design process [i.e., $\beta = 0$ in Eqs. (17)] and no uncertainty was assumed in the first five

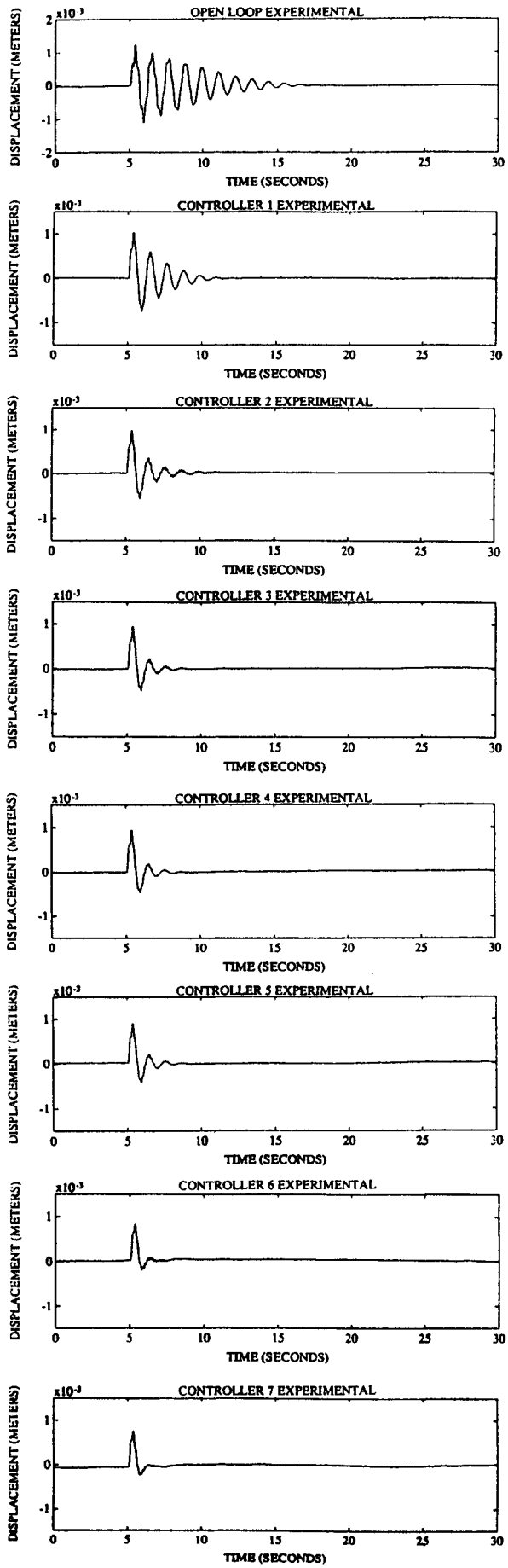

Fig. 8 Open- and closed-loop responses of displacement A of bay 18 for the decentralized controllers (controllers 1-4) and the centralized controllers (controllers 5-7).

modes. The controller was of order 25. This centralized controller yielded significantly better performance than the highest performance obtained by a decentralized controller.

Controller 7: Final Reduced-Order Linear Quadratic Gaussian Controller Using Bay 10 and Bay 18 Accelerometers

This controller used the same four sensors and two actuators as controller 6. The design process was essentially identical to that of controller 6 except that α and β in Eqs. (17) were chosen so that $\beta/\alpha = 5$. The controller was of order 33. This controller yielded the best performance of any of the decentralized or centralized controllers that were implemented.

The increasing performance improvement of controller 4 (the highest performace decentralized controller) and controllers 5-7 is shown in Fig. 8 by viewing the response of displacement A of bay 18. These responses are very close to the predicted performance.

VIII. Discussion

This experiment successfully demonstrated high-performance control law design and implementation for the Mini-MAST test bed, a flexible structure that has features representative of future spacecraft. The controllers were designed using LQG and full-order maximum entropy design and balanced controller reduction in conjunction with a precompensation methodology.

The precompensation methodology used in this experiment allows the designer to use classical insights to precompensate the original plant model at the inputs and outputs to develop a "nice" design plant for modern control design. The precompensation is appended to the modern controller to obtain the controller that is to be implemented. In this experiment, the precompensation was chosen to provide high-frequncy rolloff (i.e., robustness with respect to unstructured uncertainty) and was also used to make the design plant appear to have rate sensors and torque inputs. This precompensation methodology allows the designer to obtain controller configurations that might be difficult or impossible to obtain using straightforward applications of modern control theory. This strategy appears to be a useful means of integrating classical control concepts with modern control. In fact, it has already proven useful in designing controllers for an important benchmark problem.

The control design and implementation approach used was to start with simple controllers (i.e., reduced-order controllers, decentralized controllers, and/or controllers using relatively few sensors and actuators) and increase controller complexity to increase performance. This strategy was effective. The first four controllers each had a decentralized structure. The first controller was our simplest and did achieve some performance improvement. As the complexity of the controllers was increased by first adding order and then using additional sensors and controller order, the performance progressively improved. The performance was further improved by allowing the controllers to have a centralized structure.

Acknowledgments

We thank Keith Belvin, Anne Bruner, Sharon Tanner, Jeff Sulla, and David Geyer for their cooperation during this project. Without them, this project would not have been successful. This work was sponsored by the National Aeronautics and Space Administration under Contract NASA-18872.

References

[1]Collins, E. G., Jr., Phillips, D. J., and Hyland, D. C., "Design and Implementation of Robust Decentralized Control Laws for the ACES Structure at the Marshal Space Flight Center," *Proceedings of the American Control Conference,* IEEE, Piscataway, NJ, 1990, pp. 1449-1454.

[2]Collins, E. G., Jr., Phillips, D. J., and Hyland, D. C., "Robust Decentralized Control Laws for the ACES Structure," *Control Systems Magazine,* April 1991, pp. 62-70.

[3]Hyland, D. C., "Maximum Entropy Stochastic Approach to Controller Design for Uncertain Structural Systems," *Proceedings of the American Control Conference,* IEEE, Piscataway, NJ, 1982, pp. 680–688.

[4]Bernstein, D. S., and Hyland, D. C., "The Optimal Projection/Maximum Entropy Approach to Designing Low-Order, Robust Controllers for Flexible Structures," *Proceedings of the IEEE Conference on Decision and Control,* IEEE, Piscataway, NJ, 1985, pp. 745–752.

[5]Collins, E. G., Jr., and Richter, S., "A Homotopy Algorithm for Synthesizing Robust Controllers for Flexible Structures Via the Maximum Entropy Design Equations," *Third Air Force/NASA Symposium on Recent Advances in Multidisciplinary Analysis and Optimization,* Aerospace Structures Information Analysis Center, Dayton, OH, 1990, pp. 324–333.

[6]Bernstein, D. S., and Hyland, D. C., "Optimal Projection for Uncertain System (OPUS): A Unified Theory of Reduced-Order, Robust Control Design," *Large Space Structures: Dynamics and Control,* edited by S. N. Atluri and A. K. Amos, Springer-Verlag, New York, 1988.

[7]Bernstein, D. S., and Hyland, D. C., "The Optimal Projection Approach to Robust, Fixed-Structure Control Design," *Mechanics and Control of Space Structures,* edited by J. L. Junkins, AIAA, Washington, DC, pp. 237–293.

[8]Yousuff, A., and Skelton, R. E., "A Note on Balanced Controller Reduction," *IEEE Transactions on Automatic Control,* Vol. AC-29, No. 3, 1984, pp. 254–256.

[9]Pappa, R., Miserentino, B., Bailey, J., Elliot, K., Perez, S., Cooper, P., and Williams, B., "Mini-MAST CSI Testbed User's Guide," NASA, March 1989.

[10]Haddad, W. M., and Bernstein, D. S., "Robust Stability and Performance Analysis for State Space Systems Via Parameter-Dependent Lyapunov Functions: The Popov Criterion Revisited," *Proceedings of the IEEE Conference on Decision and Control,* IEEE, Piscataway, NJ, 1991.

[11]Francis, B. A., "A Course in H_∞ Control Theory," *Lecture Notes in Control and Information Sciences,* Vol. 88, Springer-Verlag, New York, 1987.

[12]Francis, B. A., and Doyle, J. C., "Linear Control Theory with an H_∞ Optimality Criterion," *SIAM Journal of Control and Optimization,* Vol. 25, 1987, pp. 815–844.

[13]Doyle, J. C., Glover, K., Khargonekar, P. P., and Francis, B. A., "State-Space Solutions to Standard H_2 and H_∞ Control Problems," *IEEE Transactions on Automatic Control,* Vol. AC-34, No. 8, 1989, pp. 831–847.

[14]Bernstein, D. S., and Haddad, W. M., "LQG Control with an H_∞ Performance Bound: A Riccati Equation Approach," *IEEE Transactions on Automatic Control,* Vol. 34, No. 3, 1989, pp. 293–305.

[15]King, J. A., and Irwin, R. D., "Issues in the Application of H_∞ Control to Large Space Structures," *Proceedings of the Southeastern Symposium on System Theory,* IEEE Computer Society, Los Alamitos, CA, 1990.

[16]Clar, P. G., Carrier, A., and Bryson, A. E., Jr., "Comparison of Two Methods for Causing Roll-Off in Control System Design," *Proceedings of the AIAA Guidance, Navigation, and Control Conference,* AIAA, Washington, DC, 1990, pp. 1734–1741; also, AIAA Paper 90-3580, Aug. 1990.

[17]Doyle, J. C., "Structured Uncertainty in Control System Design," *Proceedings of the IEEE Conference on Decision and Control,* IEEE, Piscataway, NJ, 1985, pp. 260–265.

[18]Balas, G. J., Chu, C.-C., and Doyle, J. C., "Vibration Damping and Robust Control of the JPL/AFAL Experiment Using μ-Synthesis," *Proceedings of the IEEE Conference on Decision and Control,* IEEE, Piscataway, NJ, 1989, pp. 2689–2694.

[19]Gupta, N. K., "Frequency-Shaped Cost Functionals: Extension of Linear-Quadratic-Gaussian Design Methods," *Journal of Guidance and Control,* Vol. 3, No. 6, 1980, pp. 529–535.

[20]Hefner, R. D., and Mingori, D. L., "Suboptimal Controller Design Using Frequency Domain Constraints," *Proceedings of the AIAA Guidance and Control Conference,* AIAA, New York, 1982; also, AIAA Paper 82-1567, Aug. 1982.

[21]Collins, E. G., Jr., King, J. A., and Bernstein, D. S., "Robust Control Design for the Benchmark Problem Using the Maximum Entropy Approach," *Proceedings of the American Control Conference,* IEEE, Piscataway, NJ, 1991, pp. 1935–1936.